CEAS EuroGNC 2019
"Conference on Guidance, Navigation and Control"
3-5 April 2019 @ Politecnico di Milano, Milan, Italy.

CEAS-GNC-2019-039

Qualitative Loss-Of-Control of Quadrotors

Su Jan Kieran Kersbergen, Sihao Sun and Coen de Visser

Abstract With current research in quadrotor Loss-Of-Control (LOC) being focussed on specific failure cases such as Single-Rotor Failure (SRF), the growth that is expected in the drone industry will not be able to be sustained, in regards to the safety of individuals in urban areas. Without an assurance of reliability regarding the safety of drones this is just not feasible. This work seeks to show the importance of modelling hazards such as the Vortex Ring State (VRS) to broaden the approach on solving LOC of quadrotors. Through the adaptation of the LOC definition of aircraft to quadrotors and a comparative analysis of quadrotor flights, of both the nominal and SRF configuration, a Qualitative LOC Definition (QLD) for quadrotors is created, which can be used for the identification of quadrotor LOC events.

1 Introduction

Loss-Of-Control (LOC) in aviation has received considerable attention in recent years [5], especially in manned aviation. This is not unexpected as a recent study from Boeing [8] shows that LOC has been and still is the main cause of fatalities in Commercial Air Transport (CAT) accidents world wide. 25.8 % (16) of all accidents that occured between 2007 and 2016 were caused by in flight LOC incidents. These incidents caused 45.8 % of all the fatalities. For small Unmanned Aircraft System

S.J.K.Kersbergen
Delft University of Technology, Kluyverweg 1, 2629 HS Delft, The Netherlands,
e-mail: kierankersbergen@gmail.com

S.Sun
Delft University of Technology, Kluyverweg 1, 2629 HS Delft, The Netherlands,
e-mail: s.sun-4@tudelft.nl

C.C. de Visser
Delft University of Technology, Kluyverweg 1, 2629 HS Delft, The Netherlands,
e-mail: c.c.deVisser@TUDelft.nl

(UAS) (under 55 *lbs*, approx. 25 *kg*), 35 % of the (reported) UAS crashes were due to LOC [7]. The unmanned aviation market is a strong growth industry, with a significant amount of UAS expected to be flying around urban areas. Thus, LOC is expected to become an quivalently important issue.

One of the most widely used UAS is the quadrotor. It is part of the class of multi-rotors and obtains flight through lift generation of four rotors.Most research regarding the safety of multi-rotors or quadrotors has been geared towards specific challenges e.g. loss of rotors or sensor failure, and not so much the higher level processes leading to LOC. It is expected that a definition of LOC in quadrotors will lead to more research aimed at a holistic solution for LOC prevention. A recent definition for LOC of quadrotor is presented in [7]. It is mentioned, however, that finding significant statistical data to back ideas for indicators of LOC is near impossible, as databases are currently not standardized and entries are voluntary.

Through the adaptation of the definition of LOC from CAT to quadrotors a comparative analysis of quadrotor flights, of both the nominal and Single-Rotor Failure (SRF) configuration, a Qualitative LOC Definition (QLD) for quadrotors is created. This definition is then validated through the analysis of thrust stand measurements and quadrotor test flights in a controlled test environment.

2 Background

Currently most of the research regarding quadrotor failure is aimed towards the various parts of Active Fault Tolerant Control Systems (AFTCS) [25], which has as a main objective to keep normal steady-state performance under nominal and off-nominal conditions. A general structure of an AFTCS can be seen in Fig. 1.

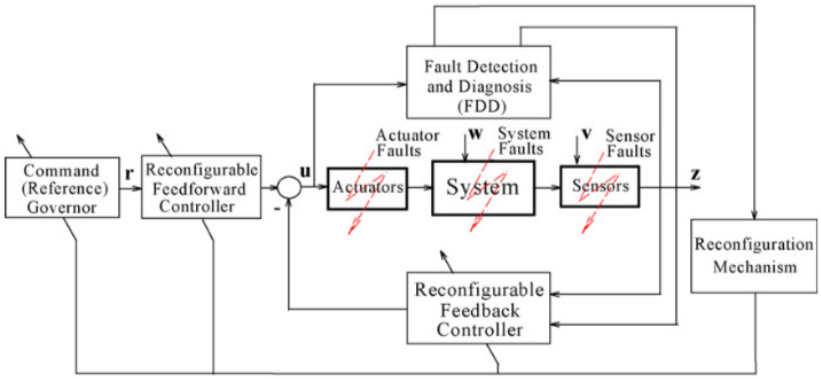

Fig. 1 General AFTCS [25]

An AFTCS system has four different sub-systems: a reconfigurable controller or Fault Tolerant Controller (FTC), a mechanism that reconfigures the controller, a Fault Detection and Diagnosis (FDD) system [1, 10, 16, 24] and a command/reference governor. The difficulties in designing a good AFTCS system are the design of: a flexible FTC, a fast and accurate FDD system and a reconfigurable mechanism. Where the first two are discussed the most in literature. Faults considered in most FTC and FDD research are sensor, actuator and structural/component failure damage [24]. LOC, however, is a higher level process with often complicated causes and effects, which for quadrotors have not been researched up to this point.

In contrast to the specific solutions in quadrotors, manned aerospace has seen a major effort into finding a holistic solution for LOC [5]. This effort was a result of the Commercial Aviation Safety Team (CAST) designating LOC as one of the three major areas of concern in CAT, in 1997. NASA and Boeing jointly developed a set of five envelopes related to aircraft flight dynamics, structural integrity, flight control and aerodynamics. Through the use of the generally accepted characteristics of LOC, see Fig. 2, they found the primary causes for LOC, from the research of the JSAT [13], derived the most important variables related to these causes, and such created the envelopes.

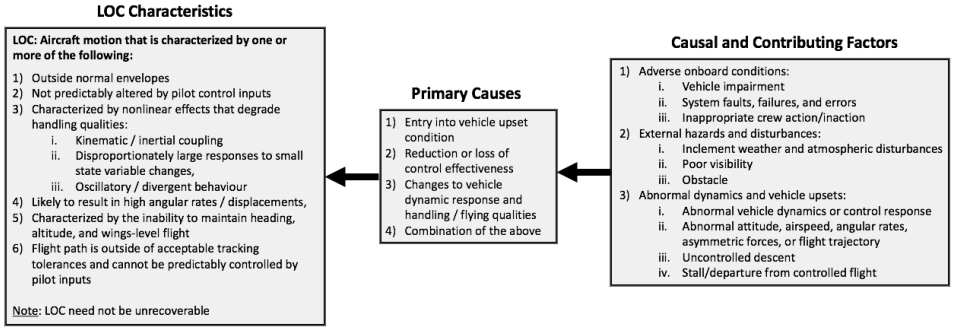

Fig. 2 CAT LOC Characteristics [4]

The envelopes gave a quantitative description to LOC, which addressed 95% of the CAST LOC cases. This tool enabled investigators to consistently define LOC cases and identify viable solutions for their reduction. These solutions have been and still are being consistently reviewed and summarized by NASA [4, 5].

Quadrotor research of this kind, has not been done. Recently however, a preliminary risk assessment and hazard identification analysis for UAS was done by the same group that had been publishing reviews on LOC of CAT [3, 7]. A key finding in their research was that a lack of standardized reporting of incidents led to situations in which meaningful analyses of data was hard. Also hazards identified for aircraft were found to not neccessarily be translatable to UAS. The general consensus was that there is just not enough qualitative data for hazard identification, this was backed by the lack of literature about statistics on quadrotor failure, like [23].

Helicopters have also not seen a quantification for LOC, although 'LOC-like' emergencies and hazards have been defined [9]. Examples of such cases are: (1) autorotation, (2) the height/velocity diagram, (3) dynamic roll over, (4) settling with power, also known as the Vortex Ring State (VRS), and (5) retreating blade stall. As the quadrotor is a simplified helicopter with four rotors, the failures and the dynamics that govern the helicopter state can also be partly applied to quadrotors. The most applicable rotorcraft hazards to the quadrotor are autorotation, which in theory is not possible due to their fixed pitch rotors and the last two examples which have been thoroughly discussed in literature [11].

The Safe Flight Envelope (SFE) is a term used loosely in literature as a means to quantify state-limitations of aircraft [26].In manned aviation it commonly refers to a region of the state-space in which the aircraft can be safely maneuvered. When it leaves this region, it reaches a state from which returning to a trim state takes a significant amount of time, or is even impossible. The SFE estimation problem can be formulated as a reachability problem [18]. It is hypothesized in this paper that the SFE provides a powerful conceptual framework for quantifying quadrotor LOC.

3 Data Analysis

To find a Qualitative LOC Definition for quadrotors, characteristics of LOC of quadrotors were defined. As the description of the characteristics of LOC of CAT is widely applicable to other vehicles, with minor changes, the following description of LOC characteristics of quadrotors is created, see Fig. 3.

LOC Characteristics

LOC: Quadrotor motion that is characterized by one or more of the following:

1) Outside normal envelopes
2) Characterized by nonlinear effects that degrade handling qualities:
    i. Kinematic / inertial coupling
    ii. Disproportionately large responses to small state variable changes,
    iii. Oscillatory / divergent behaviour
3) Likely to result in high angular rates / displacements,
4) Characterized by the inability to maintain heading, altitude, and rotors-level flight
5) Flight path is outside of acceptable tracking tolerances and cannot be predictably controlled

Note: LOC is not necessarily unrecoverable

Fig. 3 Quadrotor LOC Characteristics, Adapted from [6].

The characteristics were used in a comparative data analysis performed on flights flown with a Parrot Bebop 2 in the Open Jet Facility (OJF) (windtunnel). Out of the 110 flights, flown up to wind speeds of 16 m/s, preliminary categories and groups

were created from the 62 crashed flights, three of which did not have sufficient data. The two main groups: the nominal (32) and SRF (27) groups were both split into translational and vertical flights. Finally the SRF groups were further divided based on the rotor state: Left/Right Back (LB/RB) removed or Idle Rotor (IR).

The preliminary categories provided a good basis for incident comparison. Each preliminary category was separately analysed, where time histories of all on-board variables and windspeeds were explored per incident, compared to other incidents in the same category and grouped if similarities occured. After all the preliminary categories were analysed, cross-category similarities were sought for and grouped. Through this method the most frequent events became evident:

- **Failure/Malfunction During Descent (DD)**
  This category was only seen in SRF configuration flights, which is strange as this category is suspected to be caused by the VRS [17].
  Properties: Negative vertical speed, forward speed, angle of attack
- **F/M During Ascent (DA)**
  This category was seen sparsely, though mostly during the flights in SRF configuration, it is also suspected to be caused by the VRS, but after recovery.
  Properties: Positive vertical speed, forward speed, angle of attack
- **Phi Spike (PS)**
  A spike in the roll angle was seen at the end of a few flights. This was probably caused by the control system trying to recover from an unrecoverable situation and spiking the roll angle.
  Properties: Near crash, high roll rate reference
- **Theta Spike (TS)**
  The theta spike was also seen at the end of a few flights and was probably caused by the control system trying to recover from an unrecoverable situation. In some cases this spike, increased the angle of attack and thus exposed a greater surface area to the wind causing the crash.
  Properties: Near crash, high pitch rate reference
- **Inscreasing Oscillation of Acceleration (IO)**
  The increased oscillation of translational, vertical and angular accelerations was seen in translational flight of SRF configuration flights. An increasing wind speed is seen as the main reason for the increase in oscillations.
  Properties: Increasing velocity, wobble angle and angle of attack
- **Actuator Saturation (AS)**
  As derived from the reduced model, actuator saturation seems to be one of the major reasons for failures. Furthermore as expected it is postively correlated to the velocity and thus to the angle of attack.
  Properties: Increasing velocity, angle of attack, rotation speeds
- **High Velocity (HV)**
  High forward/wind speed caused an increase in rotor speeds, which usually led to actuator saturation and thus ultimately to failure.

Properties: Increased angle of attack, actuator saturation, slow descent

- **Slow Descent (SD)**
  Seen at high velocities, probably caused by the fact that the velocity is too much for the quadrotor to handle. Thus the thrust vector is angled more into the wind and height is lost in the process.
  Properties: High velocity, angle of attack, close to crash

- **Equipment Failure (EF)**
  Failures due to equipment e.g. actuator failure, battery low and screws loose.
  Properties: Equipment not optimal

Note that the VRS was not added to the categories as it was not apparent that the state was active or not. Its indicators were however added to the categories i.e. Failure/Crash During Descent, Failure/Crash During Ascent and the Phi/Theta Spikes. The distribution of the categories over the flights can be seen in Fig. 4.

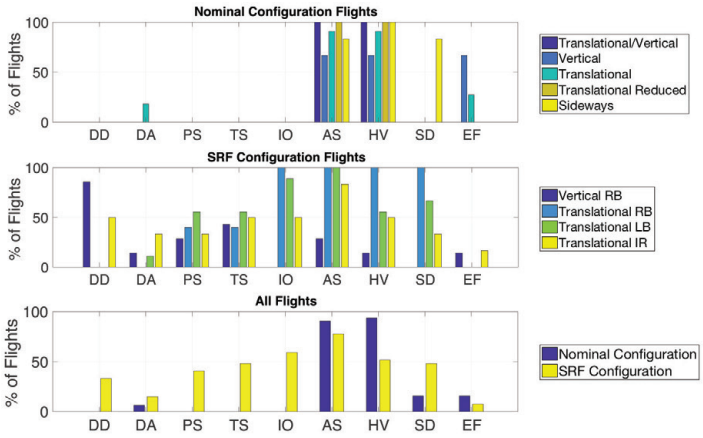

Fig. 4 Distribution of Incident Categories over the Flights

As the categories had overlapping features, they were integrated and delimited, to create a more coincise theory.

The first four categories, DD, DA, PS and TS are the indicators of the VRS [9, 17]. They were exclusively seen in the SRF configuration flights. The expectation was that these categories would also be seen in vertical nominal configuration flights, but none of the flights crashed during descent or ascent, though one flight without wind showed some instabilities during descent. Furthermore the DD category happened more often then the DA category, which was expected as VRS happens due to descent into ones own turbulence, note that the DA category usually occured right after descent. As these categories are connected through theory

and were mostly seen in combination with each other they were combined into the Vortex Ring State category.

The IO category was also only seen in the SRF configurations, where an increase in wind speed caused an increase in oscillations of the accelerations. As this was not seen in the nominal configuration this oscillation is expected to be caused by the control strategy for quadrotors in SRF configuration [19]. This strategy led to a new aerodynamic phenomenon: Double Blade Flapping (DBF), that was observed during test flights (see Sub-Section 3.B). The phenomenon causes the control system to command different rotor speeds for each rotor based on their location w.r.t. the centre of gravity and is seen as the cause of the oscillations. Thus the IO category was combined with the HV category into the Blade Flapping category.

AS and HV are the categories that were seen the most, thus they are seen as the main causes for quadrotor failures in both the configurations. Furthermore, the SD category was seen frequently in combination with the two. What was observed is that in high wind speeds more thrust was needed to hold position and therefore more actuator saturation cases were observed at those speeds. Also slow descents were observed due to the quadrotor needing to tilt its thrust vector into the wind to keep its position. As HV can be seen as a cause of other categories it was decided to combine it with AS and SD into the Actuator Saturation category.

The final category, EF, although not seen that frequently always caused dangerous situations. From empty/broken batteries causing random landing sequences or thrust spikes to actuators breaking causing uncontrolled crashes. Thus it was decided that the Equipment Failure category would remain unchanged.

Blade flapping is a phenomena seen in helicopter flight, where the advancing side of the rotor disk sees a higher effective velocity with respect to the air than the retreating side. This difference creates an offset in lift between the two and thus effectively flaps the blades up and down once per revolution [15]. Due to the symmetry of quadrotors, the lateral effects of blade flapping are cancelled. However, in the translational motion the rotor disk is tilted away from the direction of motion, and thus damped, furthermore the effective upwards thrust is lowered [11].

As the flapping angle was not measured during flight, its influence on the thrust remains unknown. However in the SRF configuration an interesting phenomenon was seen. The commanded and observed rotor speeds of the quadrotor were oscillating with the location of the rotor in the yaw plane. It was observed that a second flapping plane was created due to the SRF control strategy, see Fig. 5, where the plots show the rotor speeds of each rotor over a single flight. The red and blue half circles indicate the phase of the yaw of the quadrotor in which the respective rotor is in, the advancing side (red) and retreating side (blue). Finally the black lines show the incoming wind direction.

A rotor in the right half of the rotation plane would have more effective velocity due to the SRF control strategy [19]. Consequently, a rotor in the left half plane would have less effective velocity, thus causing a rolling moment. This rolling tendency was not observed in the experiments, the lack of observation was theorized to be caused by the control system changing the rotation speeds of each individual

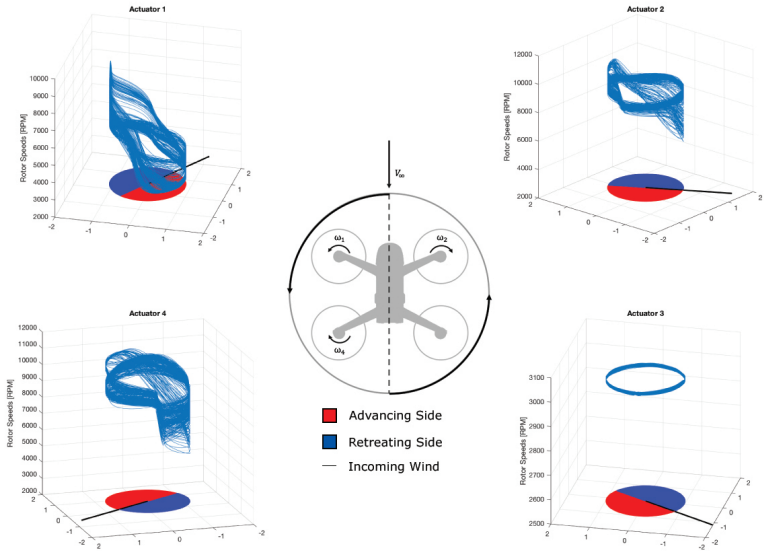

Fig. 5 Double Blade Flapping (3^{rd} rotor Removed)

rotor based on their location within the rotation plane. The rotor opposite to the removed rotor, with minimum rotation speed hardcoded to 3000 rpm, is commanded to counter the rolling moment through increasing the rotation speed in the retreating side and decreasing the rotation speed in the advancing side. This phenomenon, named Double Blade Flapping, was observed in multiple flights where it was always seen in the rotor opposite to the removed rotor.

The behaviour seen in the two (working) rotors opposite of each other also showed similar behaviours in multiple flights, where the rotor speeds would be observed to be identical. This difference in expected behaviour could have multiple sources e.g. wobbling angle, symmetry, translational velocity and the aerodynamic moments due to the different planes of the rotors and the centre of gravity. Thus this phenomenon should be further investigated.

4 Thrust Experiment

To validate the primary causes and precursors to quadrotor LOC a thrust experiment was designed to measure the thrust produced by the Parrot Bebop 2 actuator and rotor under all possible flight conditions. The following variables were identified:

- **The Angle of Attack, α:**
  To measure all flight circumstances the thrust was measured from 0 to 90 deg for both positive (upwards) and negative (downwards) velocities, see Fig. 6.

- **The Advance Ratio, J:**
  A ratio used for propellers in aeronautics and hydrodynamics to show the ratio between the freestream fluid speed and the propeller. Where the velocity is defined positive in upwards motion and negative in downwards motion.

$$J = \frac{\mathbf{V}}{n \times D} \tag{1}$$

  Where $\mathbf{V}$ is the total velocity vector, n is defined as the rotation rate of the rotors in rotations per second and D is the rotor diameter in meters.

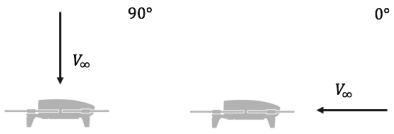

Fig. 6 Angle of Attack Definition

- **The Thrust Coefficient, C_t:**
  The dimensionless coefficient of the thrust produced by the rotor.

$$C_t = \frac{T}{\rho n^2 D^4} \tag{2}$$

  Where T is defined as the thrust, ρ is defined as the density of air, assumed to be $1.225\ kg/m^3$, and n and D are defined as in Eq. 1.

For the acquisition of the data, the dynamometer series 1580 of RcBenchmark was used. The thrust and the rotation speed were measured with a frequency of 10 Hz. Finally the wind was extracted from the OJF control system.

For each test run, the angle of attack and the velocity were kept constant, while the rotor was varied over rotational values of $3,000$ to $12,000\ rpm$ in increments of 1000 rpm. For each rotational value 50 data points were acquired, leading to 500 data points per run. The angle of attack was then varied from 0 to 90 deg in increments of 10 deg and the velocity was varied from 0 to 16 m/s in increments of 2 m/s. To do measurements on descending flight, the rotation direction and the rotor were both flipped to measure the thrust produced in descending flight.

The actuator and rotor were tested for 1600 points, where each point had 50 thrust measurements. The thrust at each data point was taken to be the average of the 50 measurements. By taking 50 measurements per point the expected thrust fluctuations could be identified [17].

As the thrust stand was close to the rotor itself a slight influence was expected. Therefore the measurements were taken after setting all values to zero on the device (tare), this however would also remove the influence of the rotor itself, therefore

extra measurements were made without setting the values to zero on the device. Furthermore the thrust stand was tested separately to test its influence. The following assumptions were made:

$$F_{notare} = F_{tare} + F_{static} \tag{3}$$

$$F_{real} = -F_{notare} + F_{testbench} \tag{4}$$

Where F_{notare} in Eq. 4 has flipped signs for the descending tests and F_{static} equals all the static forces:

$$F_{static} = F_{testbench} + F_{rotor} \tag{5}$$

For zero degrees, perpendicular to the windtunnel, there was hardly any difference between the non-tared approximate (Eq. 3) or the actual non-tared measurement, but the higher the angle of attack the bigger the difference became, where the non-calibrated measurement showed higher values of thrust. As preliminary results showed lower thrust values than the flight data, the decision was made to use the non-tared measurement.

To fit the obtained data multivariate B-splines were used. [20, 21, 22]. In Fig. 7 the triangulation used to discretize the state-space can be seen, which used the 5^{th} order polynomials over each simplice with 0^{th} order continuity (S_0^5).

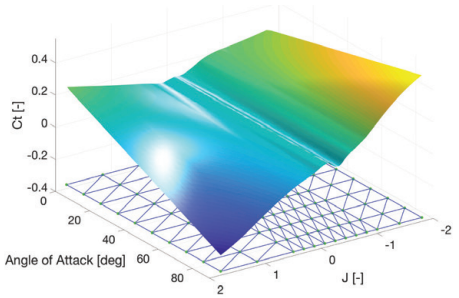

Fig. 7 Triangulation and Thrust Model

To validate the fit of the thrust model the variance of the B-coefficients was examined, furthermore a residual quality analysis was performed. Firstly the dataset was split in two separate data sets: the identification dataset and the validation dataset. The identification dataset was then used to identify the model and the validation dataset was then used to validate it.

The final model had an average B-coefficient variance of 0.0011, a Root Mean Square (RMS) error of 0.0004 and a relative RMS error of 0.19%, where the relative RMS error is defined as the RMS of the error over the RMS of the validation model.

To validate the model, it was compared to flight data. An external motion capture system (Optitrack), was used to obtain the velocity of the quadrotor. The velocity per rotor was determined through Eq. 6, where $\overrightarrow{\Omega}$ is the rotation velocity vector consistent of p, q and r, $\overrightarrow{r_i}$ indicates the location of the i^{th} rotor w.r.t. the centre of gravity and $\overrightarrow{V_{tot}}$ is the total velocity of the quadrotor.

$$\overrightarrow{V_i} = \overrightarrow{\Omega} \times \overrightarrow{r_i} + \overrightarrow{V_{tot}} \tag{6}$$

The thrust coefficient, advance ratio and angle of attack were determined through their definitions given in Eqs. 1 and 2. Where the thrust was determined through Newton's first law and the local velocity and rotor speeds were used to determine the C_t values per rotor.

In Fig. 8 the comparison between the flight data and the model data can be seen, where the dataset is split up in four manoeuvers : (1) vertical, (2) transverse, (3) longitudinal and (4) yaw changes while holding position. Where manoeuvers (1) & (2) were performed at yaw angles of 0 to 90 deg. To compare the Ct value of the whole quadrotor to the data obtained from the model both sets were z-normalised, thus the datasets indicate the standard deviations with respect to the mean of the respective set. Note that the modeldata was multiplied by 1.3 to achieve the current results, this offset of 30% is expected to have been caused by aerodynamic effects [2], which were not taken into account in the model.

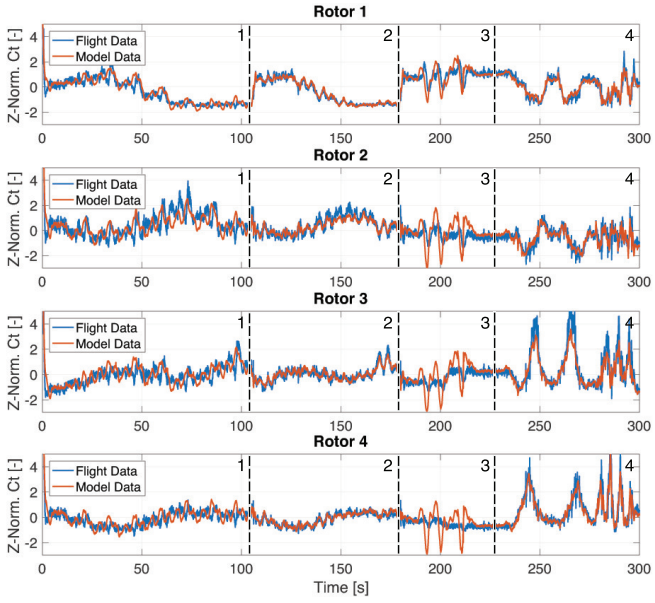

Fig. 8 Z-Normalised Nominal Configuration Flight Data & Model Data, V = 8 m/s

5 Validation

The validated thrust model was used to validate the categories and observations that were found through the data analysis, see Section 3. Where actuator saturation is seen as the primary cause to LOC events of quadrotors and the other categories and observations are seen as precursors. As the model was created for a single rotor, the aerodynamic influences of rotors on each other will not be discussed.

5.1 Vortex Ring State

From multiple sources the VRS is seen as a regime where momentum theory fails, as it is essentially the state in the flight regime where the windflow is reversed in direction. In this flight regime, the thrust is expected to be fluctuating [17].

To find the thrust variation over the flight regime of the actuator the 50 measurements per data point were used. The minimum and maximum values per data point were obtained and their difference was taken as variation. The variation was obtained for all the data points of the thrust model and can be seen in Fig. 9(a).

One can see that the thrust fluctuates in a single area in the flight regime. The thrust fluctuations in that area range up to $\pm$ 20% of the average thrust experienced in the model. Furthermore it can be seen that for higher angles of attack the fluctuation is highest. When the area is plotted over the thrust model, see the hatched area in Fig. 9(b), one can see that this area actually corresponds to the dip in thrust coefficient that is observed around an advance ratio of -0.3, see Fig. 7. Note that the hatched area shows thrust fluctuations of more than 3%.

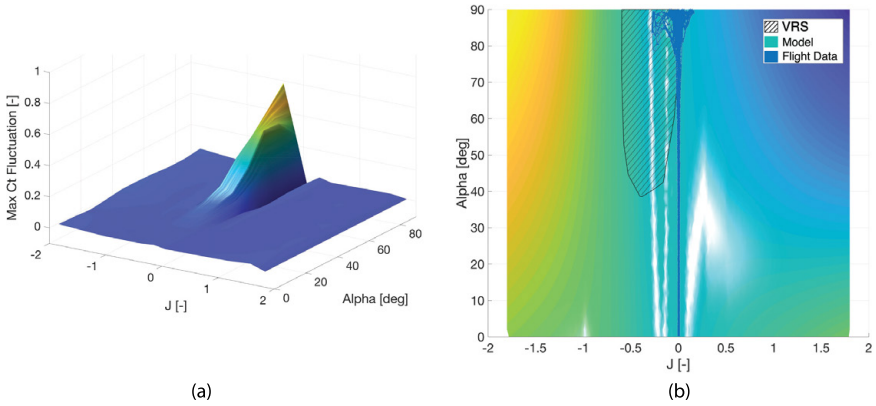

Fig. 9 **(a)** Thrust Model C_t Fluctuation, **(b)** Thrust Fluctuation and VRS Flight on Thrust Model

As the location of the dip in thrust, with respect to the thrust model, and the observed fluctuation of thrust values were what was expected from literature, this

area is seen as part of the flight regime where one encounters the VRS. Thus one can conclude that when descending it is best to have some translational velocity, to minimize thrust fluctuation. In amateur flight, translational movement is also known as a way to counter the "Wobble of Death".

One flight, in nominal configuration, was flown with the intention to maximize descent velocity with minimum forward speed. The only indication of the expected instability that was seen, was a slight wobble when stabilizing after dropping from maximum height. Therefore the assumption was made that the descent velocity was not high enough to reach the VRS.

The flight was projected over the thrust model in Fig. 9(b). One can see that according to the model the VRS was reached. Contrary to the assumption made, the descent velocity was high enough. The area with the highest thrust fluctuation was even reached, which corresponds to $\pm$ 20%. However, the time history of the manoeuver only showed a thrust reference error of 1.5%, where overall in the flight the reference error fluctuated between $\pm$ 0.25%. This could be caused by various factors such as time in descent, influence of the control system and sudden sidewinds, which are frequently discussed in the amateur scene. For further validation, experiments should be performed in the heart of the VRS area, possibly from higher heights.

5.2 Blade Flapping

As the experiment only produced vertical thrust, it was not possible to directly extract flapping angles. To investigate the effect of blade flapping, the hinged blade model suggested in [14] was used to estimate the blade flapping angle:

$$\alpha_{fl} = \frac{1}{1+\frac{\mu_{lon}^2}{2}} \frac{4}{3} \left(\frac{C_t}{\sigma} \frac{2}{3} \frac{\mu_{lon}\gamma}{a_0} + \mu_{lon}\right) \tag{7}$$

Where a_0 is the lift curve per radian, which is approximately 6.0 for conventional airfoils at low Mach numbers [15]. In Eq.8 μ_{lon} is defined as the longitudinal velocity to tip speed ratio, σ is defined as the solidity ratio, which is the area of the rotor surface covered by rotor blades and γ is the non-dimensional Lock number, which gives the ratio between aerodynamic and centrifugal forces, where I_b is the moment of inertia of the blade about the hinge and c is the chord of a blade.

$$\mu_{lon} = \frac{v_{lon}}{v_t}, \quad \sigma = \frac{A_b}{A}, \quad \gamma = \frac{\rho a_o c R^4}{I_b} \tag{8}$$

The flapping angle is then used to determine the percentage of lost thrust due to flapping (Eq. 9), where T_{meas} is the force perpendicular to the original blade:

$$T_{loss} = \left(1 - \frac{T_{meas}}{T}\right) \times 100 = (1 - \cos\alpha_{fl}) \times 100 \tag{9}$$

The results of the hinged blade model can be seen in Fig. 10, where one can see the flapping angle with respect to the angle of attack and the advance ratio and the thrust loss. The flapping angle goes up to a max/min of $\pm$ 40 degrees and the thrust loss reaches up to 25%. Note that normal flights occur between $\pm$ 0.8 J, in which more plausible values are seen. To make up for the loss of thrust, rotor speeds need to be increased, thus causing a higher probability of rotor saturation. As the results were very sensitive to the moment of inertia of the blade about the hinge, it is recommended that the results of the model be validated.

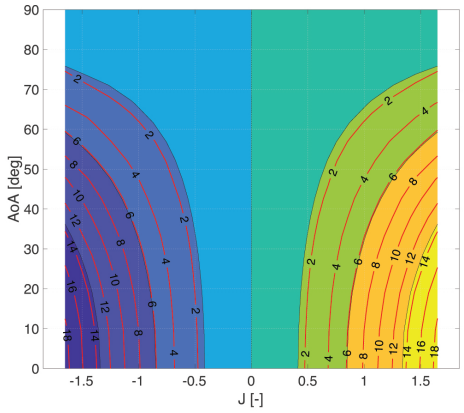

Fig. 10 Flapping Angle [deg] and Thrust Loss [%]

5.3 Rotor Saturation

The limitations of the actuators of the Bebop 2 are 3000 and $\pm$ 11000 rpm. Where the minimum limit is hardcoded, and the maximum limit was found through experiments. In Fig. 11 one can see the distribution of the advance ratio indicated in steps of 0.1 J, where the red lines indicate steps of 0.5 J.

In App. 1 data of the flights that were flown in both the nominal and SRF configuration are projected on the flight regime, that was used for the thrust model, to give an indication of the range the quadrotor can reach in different configurations and under various circumstances. Note that these projections are the data sets of the first rotor, where in the nominal case the other rotors show similar behaviour.

From the nominal configuration flights (App. 1) it can be seen that the advance ratio varied between $\pm$ 0.8 J, where, in combination with Fig. 11, it can be seen that the limit of 0.8 J at 14 m/s is a lower limit of 7000 rpm. From the advance ratio ranges observed for the other velocities, it can be seen that the maximum advance ratio flown in each flight speed is limited by the minimum rpm and thus consequently the minimum advance ratio is limited by the maximum rpm. Thus the maximum

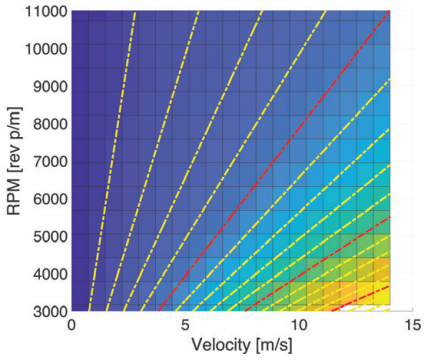

Fig. 11 Advance Ratio Distribution

attainable advance ratio for nominal quadrotors is dependent on the minimum rpm that can stabilize the quadrotor at a given velocity. This minimum value increases with the velocity, which consequently increases the angle of attack and the flapping angle. This eventually leads to the minimum rpm exceeding the maximum rpm, thus one can conclude that the nominal configuration is limited by rotor saturation.

As with the nominal configuration flights only the first rotor datasets were projected on the flight regime used for the thrust surface (App. 1). However, contrary to the rotors of the nominal configuration, the rotors of the SRF configuration did not show similar behaviour, see Fig. 12. As the SRF configuration uses high-speed spinning relaxed hovering solutions [12], this was to be expected. Note that the flights in the SRF configuration do not include a legend, as the pattern of the SRF configuration flights is more dependent on the wobbling angle than the wind speed.

The SRF configuration reaches higher angles of attack and higher advance ratio values in the rotor opposite to the failed rotor. This increase is caused by the wobbling angle that increases with the tilt of the primary-axis. Increasing the tilt of the primary-axis in the direction opposite to the failed rotor also lowers the energy needed to keep wobbling and thus the rpm of the remaining rotors (two and four) are lowered. Note that there is an optimum in trading rpm speeds between the rotors.

It can be observed that the higher advance ratio values seen in the SRF configuration all occur in the rotor opposite to the failed rotor. Furthermore the remaining rotors have similar, but mirrored patterns. This pattern was also seen in the DBF phenomenon. Due to the increased effective velocity on the advancing side and the lowered effective velocity on the retreating side the rotor opposite to the failed rotor sees a greater fluctuation in rotor rpm, where the minimum rpm is the cause of the increased advance ratio. Thus as with the nominal configuration, the maximum advance ratio of the SRF configuration is determined by the minimum rpm needed to stabilize at a given velocity and therefore it is also limited by rotor saturation.

Finally the vertical flights in the SRF configuration also touched upon the VRS domain. As 80% of the SRF configuration test flights showed crashes during descending vertical flight, this could likely be due to the thrust variation in the VRS. Where the prime suspects for rotor saturation are the second and fourth rotor as they

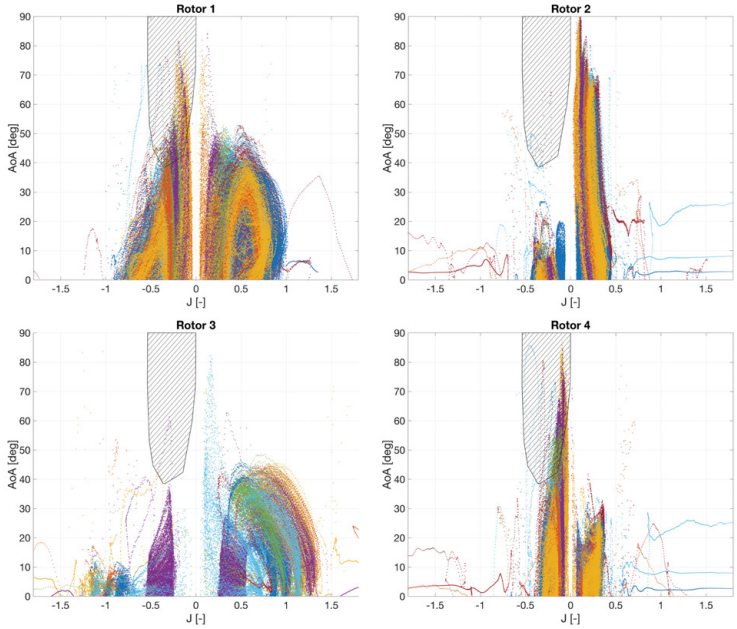

Fig. 12 Vertical Flights of Quadrotors in SRF Configuration (3^{rd} Rotor Removed)

see higher rotation speeds then the first rotor. Note that this assumption changes when the quadrotor rotates in the opposite direction and/or a different rotor fails.

6 Conclusion

The Qualitative Loss-Of-Control Definition (QLD) for quadrotors is similar to the definition given to LOC of CAT, but where the CAT have multiple upset conditions, the quadrotor only has one: actuator saturation. Furthermore a difference is seen in the dynamic and equipment failure precursors. The definition of the QLD can be found in Fig. 13. Hazards, which are currently unlikely to occur, such as the hazards under the ”Inclement Weather & Atmospheric Disturbances”, were also added as they are likely to occur when quadrotors will eventually be used for longer flights over greater distances.

As the two major sub-systems of the AFTCS, the FTC and FDD, are often researched separately in literature and have not been successfully unified, actuator failure has not been added to the primary causes. Once the AFTCS has been completed and actuator failures have become survivable, it should be added. In case the QLD is adapted to multicopters it could be immediately added, as multicopters,

that have more rotors than the quadrotor, have inbuilt redundancy and are therefore resistant to actuator failure.

With a QLD for quadrotors defined, investigators of LOC events of quadrotors have a valuable tool to be able to label/group events and thus are able to systematically seek viable safety intervention strategies to reduce the occurance of LOC.

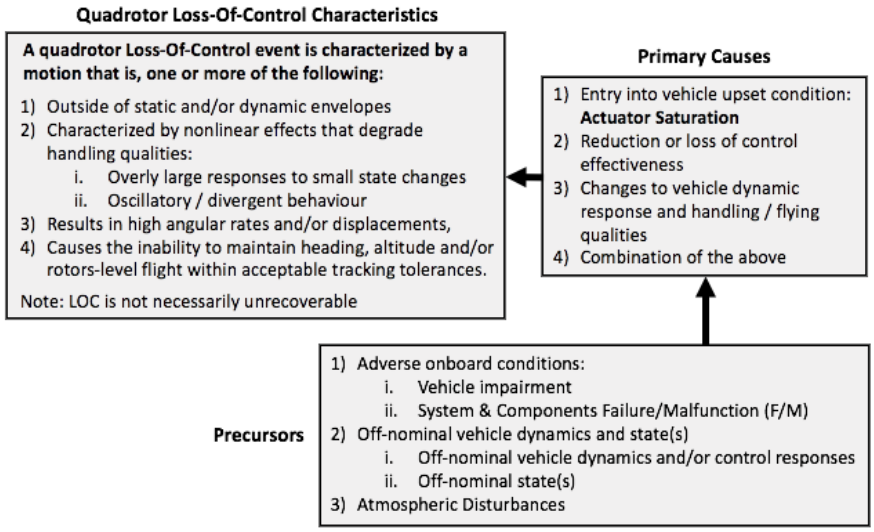

Fig. 13 Qualitative LOC Definition (QLD) for quadrotors, Primary Causes and Precursors, Adapted from CAT LOC [6]

Acknowledgements If you want to include acknowledgments of assistance and the like at the end of an individual chapter please use the `acknowledgement` environment – it will automatically render Springer's preferred layout.

References

1. Avram, R., Zhang, X., Muse, J.: Quadrotor sensor fault diagnosis with experimental results. Journal of Intelligent and Robotic Systems **86**(1), 115–137 (2017)
2. Barcelos, D., Kolaei, A., Bramesfeld, G.: Performance predictions of multirotor vehicles using a higher-order potential flow method. In: 2018 AIAA Aerospace Sciences Meeting. Kissimmee, Florida (2018)
3. Barr, L., Newman, R., Ancel, E., Belcastro, C., Foster, J., Evans, J., Klyde, D.: Preliminary risk assessment for small unmanned aicraft systems. In: AIAA Aviation Technology, Integration, and Operations conference. Denver, Colarado, USA (2017)
4. Belcastro, C.: Loss of control prevention and recovery onboard guidance, control, and systems technologies. In: AIAA Guidance, Navigation, and Control Conference. Minneapolis, Minnesota, USA (2012)

5. Belcastro, C., Foster, J., Shah, G., Gregory, I., Cox, D., Crider, D., Groff, L., Newman, R., Klyde, D.: Aircraft loss of control problem analysis and research toward a holistic solution. Journal of Guidance, Control, and Dynamics **40** (2017)
6. Belcastro, C., Newman, R., Crider, D., Klyde, D., Foster, J., Groff, L.: Aircraft loss of control: Problem analysis for the development and validation of technology solutions. In: AIAA Guidance, Navigation, and Control Conference. San Diego, California, USA (2016)
7. Belcastro, C., Newman, R., Evans, J., Klyde, D., Barr, L., Ancel, E.: Hazards identification and analysis for unmanned aircraft system operations. In: 17th AIAA Aviation Technology, Integration, and Operations Conference. Denver, Colorado, USA (2017)
8. Boeing: Statistical summary of commercial jet airplane accidents worldwide operations 1959-2016. Technical report, Aviation Safety Boeing Commercial Airplanes, Seattle, Washington, USA (2017)
9. Federal Aviation Administration: Helicopter Flying Handbook, chap. Helicopter Emergencies and Hazards, pp. 11–1 – 11–24. Oklahoma City, USA (2012)
10. Freddi, A., Longhi, S., Monteriu, A.: A model-based fault diagnosis system for a mini-quadrotor. In: Workshop on Advanced Control and Diagnosis. Zielona Gora, Poland (2009)
11. Huang, H., Hoffmann, G., Waslander, S., Tomlin, C.: Quadrotor helicopter flight dynamics and control: Theory and experiment. In: AIAA Guidance, Navigation and Control Conference and Exhibit. South Carolina, USA (2007)
12. Mueller, M., D'Andrea, R.: Relaxed hover solutions for multicopters: Application to algorithmic redundancy and novel vehicles. The International Journal of Robotics Research (2015)
13. Pardee, J., Russell, P.: Final report - loss of control jsat: Results and analysis. Technical report, Federal Aviation Administration (FAA), Washington D.C., USA (2000)
14. Pounds, P., Mahony, R., Corke, P.: Modelling and control of a quad-rotor robot. In: Proceedings of the Australasian Conference on Robotics and Automation (2006)
15. Prouty, R.: Helicopter Performance, Stability, and Control. Prindle, Weber and Schmidt (PWS Publishers) (1986)
16. R.C.Avram, Zhang, X., Muse, J.: Quadrotor actuator fault diagnosis and accomodation using nonlinear adaptive estimators. IEEE Transactions on Control Systems Technology **25**(6) (2017)
17. Shetty, O.R., Selig, M.S.: Small-scale propellers operating in the vortex ring state. In: 49th AIAA Aerospace Sciences Meeting AIAA (2011)
18. Stapel, J., de Visser, C., Kampen, E.J.V., Chu, Q.: Efficient methods for flight envelope estimation through reachability analysis. In: AIAA Guidance, Navigation, and Control Conference (2016)
19. Sun, S., Sijbers, L., Wang, X., de Visser, C.: High-speed flight of quadrotor despite loss of single rotor. IEEE Robotics and Automation Letters **3**(4) (2018)
20. de Visser, C., Mulder, J., Chu, Q.: Global nonlinear aerodynamic model identification with multivariate splines. In: AIAA Atmospheric Flight Mechanics Conference (2009)
21. de Visser, C., Mulder, J., Chu, Q.: A new approach to linear regression with multivariate splines. Automatica **45**(12), 2903–2909 (2009)
22. de Visser, C., Mulder, J., Chu, Q.: Differential constraints for bounded recursive identification with multivariate splines. Automatica **47**, 2903–2909 (2011)
23. Wild, G., Murray, J., Baxter, G.: Exploring civil drone accidents and incidents to help prevent potential air disasters. Aerospace **3**(3) (2016)
24. Zhang, Y., Chamseddine, A., Rabbath, C., Gordon, B., Su, C., Rakheja, S., Fulford, C., Apkaraian, J., Gosselin, P.: Development of advanced fdd and ftc techniques with application to an unmanned quadrotor helicopter testbed. Journal of the Franklin Institute **350**, 2396–2422 (2013)
25. Zhang, Y., Jiang, J.: Bibliographical review on reconfigurable fault-tolerant control systems. Annual Reviews in Control **32**, 229–252 (2008)
26. Zhang, Y., de Visser, C., Chu, Q.: Online safe flight envelope prediction for damaged aircraft: A database-driven approach. In: AIAA Modeling and Simulation Technologies Conference. San Diego, California, USA (2016)